CHEMISTRY

Genuine binding energy of the hydrated electron

David Luckhaus,[1] Yo-ichi Yamamoto,[2] Toshinori Suzuki,[2] Ruth Signorell[1]*

The unknown influence of inelastic and elastic scattering of slow electrons in water has made it difficult to clarify the role of the solvated electron in radiation chemistry and biology. We combine accurate scattering simulations with experimental photoemission spectroscopy of the hydrated electron in a liquid water microjet, with the aim of resolving ambiguities regarding the influence of electron scattering on binding energy spectra, photoelectron angular distributions, and probing depths. The scattering parameters used in the simulations are retrieved from independent photoemission experiments of water droplets. For the ground-state hydrated electron, we report genuine values devoid of scattering contributions for the vertical binding energy and the anisotropy parameter of 3.7 ± 0.1 eV and 0.6 ± 0.2, respectively. Our probing depths suggest that even vacuum ultraviolet probing is not particularly surface-selective. Our work demonstrates the importance of quantitative scattering simulations for a detailed analysis of key properties of the hydrated electron.

INTRODUCTION

The broad attention the hydrated electron e_{aq}^- has attracted over many decades is attributed to its important role in a wide range of fields, including radiation damage in aqueous systems (*1*–*4*), and to the fact that even though it is one of the simplest quantum solutes, several of its properties remain controversial. Substantial progress has been made in recent years regarding its structural and electronic properties (*5*–*21*) and the excited-state relaxation dynamics over a broad time window, ranging from femtoseconds to beyond picoseconds (*9*, *10*, *13*, *22*–*32*). The most controversial issues concern the ground-state structure (cavity-forming versus non–cavity-forming), the relaxation mechanisms from electronically excited states (adiabatic versus nonadiabatic), the existence of a long-lived surface electron, accurate values for electron binding energies (eBE), and the influence of electron scattering. Although evidence has been provided in favor of an s-like ground-state wave function (*11*, *15*, *17*) [presumably in a quasi-spherical solvent cavity (*11*, *15*)] and for a nonadiabatic relaxation mechanism after s→p excitation (*22*, *24*–*26*), the existence of a long-lived surface electron with distinct energetics and its potential influence on DNA damage are still discussed controversially (*6*, *9*, *13*, *14*, *16*, *27*, *28*, *33*).

A still unresolved issue concerns the influence of elastic and inelastic electron scattering on the measurement of key properties of the hydrated electron (*8*, *23*, *28*, *34*–*41*). Electron scattering determines the probing depth in photoelectron spectra of water microjets and water droplets (*35*, *42*) and is thus crucial to clarify which region of the aqueous sample—the top molecular layer, the interfacial region, or the bulk—is primarily probed. There were no reliable estimates of the probing depths for e_{aq}^- in the electron kinetic energy (eKE) region below 10 eV, and it has been only speculated to be on the order of 1nm (*7*, *8*, *23*–*25*, *28*, *34*, *36*, *37*)—which resulted in ambiguities in the interpretation of experimental data. For lack of detailed scattering data for very slow electrons in liquid water, no attempt has been made to retrieve genuine eBE spectra of e_{aq}^- [referred to in the following as $eBE^{(g)}$], namely spectra that are not distorted by scattering of the electron in the solvent (Fig. 1). This in turn has hampered the determination of vertical electron binding energies (VBEs) and the interpretation of photoelectron angular distributions (PADs). VBEs are defined as the most probable eBEs (position of band maxima) observed in the photoelectron spectra of solvated electrons. Most reported VBEs for the ground-state hydrated electron vary between 3.3 and 3.9 eV with quoted uncertainties of typically ~0.1 eV (table S1 and fig. S1) (*6*–*8*, *27*). The variation arises, in part, from the streaming potential of the liquid microjet (*43*), which has often been ignored, and from the influence of the work function difference between the liquid and the apparatus (*44*). However, a more essential problem is elastic and inelastic electron scattering in the liquid before photoemission (*8*). Without detailed scattering parameters and simulations, the actual effect of scattering remained unclear so that no genuine $VBE^{(g)}$ could be extracted from the experimental spectra. Similarly, the importance of electron scattering for the interpretation of experimental PADs was recognized (*22*, *23*, *34*, *45*), but without accurate scattering simulations, its quantification remained elusive. PADs are very sensitive to the actual values of the scattering cross sections. Isotropic PADs are expected for large elastic and inelastic electron scattering cross sections, whereas small cross sections may partly preserve the genuine photoelectron anisotropy [$PAD^{(g)}$]. Here, we combine photoelectron spectroscopy of e_{aq}^- in liquid water microjets with detailed electron scattering simulations with the aim of resolving ambiguities concerning the influence of electron scattering on key properties of the hydrated electron.

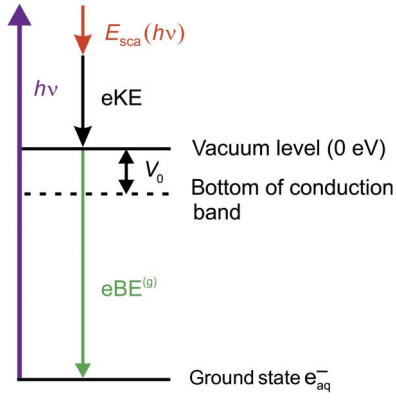

Fig. 1. Energy diagram of photoionization. The ground-state hydrated electron e_{aq}^- is ionized by the ionization laser $h\nu$. E_{sca} is the energy loss due to scattering, eKE is the recorded electron kinetic energy, and $eBE^{(g)}$ is the genuine electron binding energy (Eq. 2). V_0 is the location of the conduction band edge of water relative to the vacuum level ("escape barrier").

[1]Laboratory of Physical Chemistry, Department of Chemistry and Applied Biosciences, ETH Zürich, Vladimir-Prelog-Weg 2, CH-8093 Zürich, Switzerland. [2]Department of Chemistry, Graduate School of Science, Kyoto University, Kitashirakawa-Oiwake-cho, Sakyo-Ku, Kyoto 606-8502, Japan.
*Corresponding author. Email: rsignorell@ethz.ch

For lack of liquid water data, previous scattering simulations of the liquid bulk used scattering parameters of amorphous ice at low eKEs (*38*), which have existed for some time (*39*), whereas corresponding values for liquid water have only very recently become available through photoelectron imaging of liquid water droplets (*35*). In the past, estimates regarding the influence of scattering on the hydrated electron (*6*, *8*, *23*, *24*, *28*) were based on approximate or extrapolated values of the electron attenuation length (EAL) retrieved from water microjet studies (*28*, *36*, *40*, *41*). At an eKE of ~3 eV, an approximate EAL of ≥5 nm was suggested in an ultraviolet microjet photoemission study (*28*). Further, EAL data for eKEs below 10 eV were obtained from extrapolations of EAL data recorded at eKEs of >10 eV in soft x-ray water microjet studies (*36*, *40*, *41*). Resulting EAL values ranged from "at least a few nanometers" (*41*) to subnanometers (*36*). However, rather than the variation in the reported EALs, the major challenge arises from the fact that single quantities, such as EALs, do not allow quantitative predictions of scattering effects, which are the result of the complex interplay of various contributions. The EAL, for example, describes the average damping effect of various types of scattering events with different angular and energy loss characteristics, which cannot be extracted from EALs alone (*46*). Here, we address this issue with a detailed, probabilistic electron transport model (*35*, *39*) using our recently retrieved scattering parameters for low eKEs from the work of Signorell *et al.* (*35*). These scattering parameters were obtained from photoemission imaging measurements of water droplets (*35*) and are independent of the present liquid jet data. Our simulations explicitly take into account the cross sections, energetics, and angular-dependences of all relevant scattering processes (inelastic electron-phonon, electron-vibron, and electron-electron scattering and isotropic elastic scattering; note that forward elastic scattering does not contribute here) as well as the intensity distribution of the ionizing radiation in the microjet (see Materials and Methods, section S2, and figs. S2 and S3).

RESULTS AND DISCUSSION

Hydrated electron formation and detection

The experimental setup comprises a water microjet, a femtosecond laser system (1 kHz), and a magnetic bottle photoelectron spectrometer (fig. S4) (*8*, *23*). Hot hydrated electrons $(e_{aq}^-)^*$ are formed by charge transfer–to–solvent (CTTS) excitation of precursor anions [I^- or $Fe(CN)_6^{4-}$] at pump energies $h\nu_{pump}$ between 215 and 270 nm. After a time delay Δt of several hundred picoseconds, $(e_{aq}^-)^*$ relax to their thermalized ground-state e_{aq}^-, from which they are excited into vacuum (e^-) by the ionization (probe) laser with photon energy $h\nu$

$$(e_{aq}^-)^* \xrightarrow{\Delta t} e_{aq}^- \xrightarrow{h\nu} e^- \qquad (1)$$

The eKE distribution of the photoelectrons e^- is measured for different values of $h\nu$ between 3.6 and 13.6 eV. Experimental details are provided elsewhere (section S3) (*8*, *23*).

Influence of electron scattering on photoelectron spectra

Figure 2 (A and B) shows experimental and simulated eKE distributions, respectively, for 3.6 eV ≤ $h\nu$ ≤ 13.6 eV (fig. S5) (*8*). For all different ionization energies, the experimental spectra (Fig. 2A) are perfectly reproduced by our detailed scattering model (Fig. 2B and fig. S5). Without scattering, by contrast, the agreement with the experiment is unsatisfactory (fig. S6). The band shapes cannot be reproduced if scattering is neglected, highlighting its importance. In a sensitivity analysis of the simulations, we find virtually identical results for variations of the scattering parameters within their respective uncertainties (section S5) (*35*), indicating that robust values for binding energies, probing depths, and PADs can be derived from the simulations shown in Fig. 2.

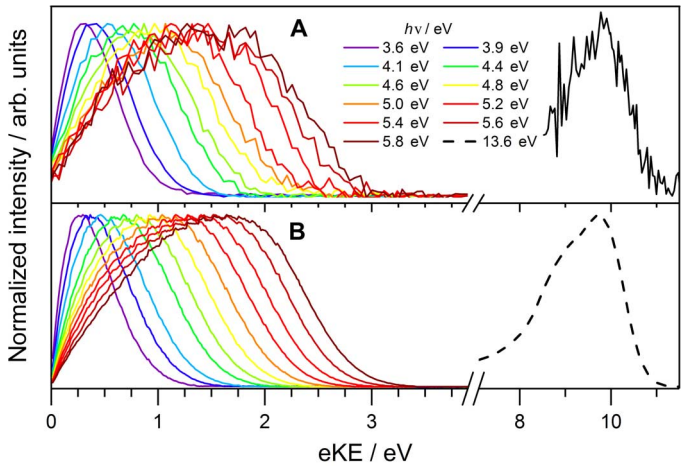

Fig. 2. Experimental and simulated photoelectron spectra of e_{aq}^-. Photoelectron kinetic energy distributions for 12 different ionization laser energies 3.6 eV ≤ $h\nu$ ≤ 13.6 eV. All spectra are normalized to the same maximum intensity. (**A**) Experimental spectra. (**B**) Scattering simulations (section S2 and fig. S5).

For ionization laser energies $h\nu$ ≤ 5.8 eV, both the experimental and the simulated eKE distribution in Fig. 2 show a pronounced dependence on the photon energy. The eKE distribution gradually shifts toward higher energy with the probe photon energy $h\nu$, as anticipated. However, the eBE distribution calculated using eBE = $h\nu$ − eKE (Fig. 3 and fig. S9) also varies with the probe photon energy, manifesting a strong influence of inelastic scattering. The position of the band maxima in the eBE spectra, that is, the apparent VBEs, increases with increasing $h\nu$, making it difficult to determine the true $VBE^{(g)}$ directly from the experimental spectra. As we have previously suggested, the true $VBE^{(g)}$ could be obscured by the influence of energy-dependent inelastic electron scattering in the liquid, leading to an apparent dependence of the experimental VBEs on the ionization energy (*8*).

Genuine electron binding energy

The present work resolves the ambiguities in determining $VBE^{(g)}$ from experimental spectra by analyzing them in terms of detailed scattering calculations. Inelastic electron scattering reduces the eKE before the escape into vacuum. Because the scattering parameters (differential cross sections and energy loss) are energy-dependent, scattering depends on the initial kinetic energy distribution and thus on $h\nu$. This leads to an additional, explicitly energy-dependent scattering correction $E_{sca}(h\nu)$ in the expression that relates measured eKEs and genuine $eBEs^{(g)}$ (Fig. 1)

$$eBE^{(g)} = h\nu - E_{sca}(h\nu) - eKE \qquad (2)$$

$E_{sca}(h\nu)$ is not a simple function of $h\nu$, but it shows a complicated $h\nu$ dependence that can only be captured by detailed modeling of the various scattering processes (see Materials and Methods, section S2, and fig. S3). Although probe energy dependencies of eBE spectra are not uncommon, particularly at the very low eKEs of interest here, our

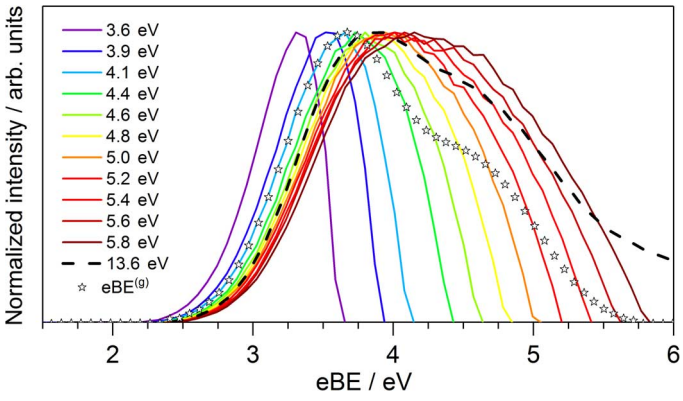

Fig. 3. eBE spectra of e_{aq}^-. eBE spectra for 12 different ionization laser energies 3.6 eV ≤ $h\nu$ ≤ 13.6 eV (lines). The stars represent the genuine $eBE^{(g)}$ spectrum; that is, the spectrum devoid of scattering contributions. The genuine $VBE^{(g)}$ is 3.7 ± 0.1 eV. For clarity, only the calculated data from Fig. 2 are shown here. See fig. S9 for a comparison with the experiment.

scattering analysis reveals as its most intriguing result the existence of a distinct genuine $eBE^{(g)}$ spectrum that is independent of the probe energy. In liquid water, the $h\nu$ dependence of eBE spectra is apparently completely described by transport properties. The genuine $eBE^{(g)}$ spectrum is shown in Fig. 3 (figs. S9 and S10) as open stars together with the eBE spectra measured for 3.6 eV ≤ $h\nu$ ≤ 13.6 eV. At this point, it remains unclear whether the asymmetric shape of the $eBE^{(g)}$ spectrum arises from initial state or final state (conduction band) contributions. The latter would reflect a structured density of final states. The fact that the shape of the $eBE^{(g)}$ spectrum does not depend on $h\nu$ makes this explanation less plausible. Alternatively, the asymmetric band shape could result from a distribution of different initial states, for example, different types of cavities with different ionization energies and different ionization cross sections. The deviations of the 12 eBE spectra from the $eBE^{(g)}$ spectrum indicate a complex dependence on $h\nu$, which arises from a combination of energy-dependent scattering and limited photon energy. The latter is primarily responsible for the narrow bandwidths and the shift toward lower VBEs (maxima) of the spectra recorded at $h\nu$ < 4.4 eV, whereas all other deviations arise from energy-dependent electron scattering. This includes the shift toward higher VBEs of the spectra recorded at $h\nu$ ≥ 4.4 eV. An increase of the most probable eBE value compared with the $eBE^{(g)}$ spectrum is expected because inelastic scattering reduces the kinetic energy, thus increasing the apparent binding energy. This shift is neither linear nor monotonous in $h\nu$. For example, the maximum of the spectrum (Fig. 3; dashed line) lies close to the maximum of the spectrum but below that of the spectrum. This is an immediate consequence of the energy dependence of scattering cross sections. The retrieval of a genuine $eBE^{(g)}$ spectrum finally allows us to determine an unambiguous value of 3.7 ± 0.1 eV for the genuine $VBE^{(g)}$ of the hydrated electron in liquid water. This value is independent not only of scattering contributions but also of the specific experimental settings (photon energy) so that the same $VBE^{(g)}$ describes the experimental spectra recorded at different ionization laser energies. A substantial part of the spread in the experimentally observed apparent VBEs (3.3 to 4.5 eV; table S1) originates from electron scattering in the liquid.

Probing depth

The complex role of scattering is also reflected in the probing depths in Fig. 4 (fig. S11). For photon energies of ≤5.8 eV, the probing depth increases with $h\nu$ because higher ionization energies result in higher eKEs. Electrons with higher eKEs can travel further away from their point of origin, which results in a larger probing depth. The nonlinear trend in the probing depths in Fig. 4 reflects the energy dependence of the scattering parameters, whereas the penetration depth of the ionizing radiation (fig. S2A) is much larger than the scattering mean free path of a few nanometers and does not affect the probing depth. This remains true at $h\nu$ = 38.7 eV, where the probing depth decreases below the value at $h\nu$ = 3.6 eV, solely as a result of scattering. The penetration depth of the ionizing radiation is still on the order of 25 nm. The influence of scattering is more pronounced at higher $h\nu$ of 38.7 eV compared with $h\nu$ of ≤5.8 eV because of electron attachment and electronic scattering channels, which come into play at eKEs above 6 eV, resulting in a much larger energy loss per scattering event (stopping power). The energy dependence of the probing depth influences the surface sensitivity of eBE spectra and their shape (fig. S12). The probing depth at $h\nu$ = 38.7 eV is of particular relevance to the question of whether a highly preferential detection of surface-bound electrons, as suggested by Siefermann *et al.* (*6*), is feasible. Unless surface-bound electrons have a much higher photoionization cross section, such a high surface sensitivity appears inconsistent with our data (fig. S11), which predict that even at $h\nu$ = 38.7 eV, 50% of the total electron signal still originates from e_{aq}^- solvated deeper in the liquid than three monolayers from the surface.

Influence of electron scattering on PAD

Finally, let us consider the influence of electron scattering on the PAD. Our recent angle-resolved liquid microjet photoemission study revealed an almost isotropic PAD for e_{aq}^- [see Fig. 4D of Yamamoto *et al.* (*23*)] at $h\nu$ = 4.8 eV. The experimentally measured anisotropy parameter was extremely small. The simulation of the minute anisotropy enabled us to derive an anisotropy parameter $\beta^{(g)}$ = 0.6 ± 0.2 for the $PAD^{(g)}$ at $h\nu$ = 4.8 eV (section S8), which is consistent with an s-like ground-state wave function of e_{aq}^- (*11*, *15*, *17*). In contrast to the liquid jet, the decrease of $\beta^{(g)}$ by scattering is almost negligible for e_{aq}^- in small water anion clusters with ~50 H_2O molecules. For this cluster (0.7-nm radius), we calculate a reduction of $\beta^{(g)}$ by less than 0.1 (fig. S14) in the same eKE range, which is in agreement with the experimental value $\beta_{cluster} \approx 0.7 \pm 0.1$ from the study of Bragg *et al.* (*45*). The value of $\beta^{(g)}$ = 0.6 ± 0.2 we drive for liquid water at $h\nu$ = 4.8 eV provides PADs that are consistent with the experimental observations, namely, isotropic PADs for e_{aq}^- in liquid microjets (*23*) and anisotropic PADs for anion clusters (*45*).

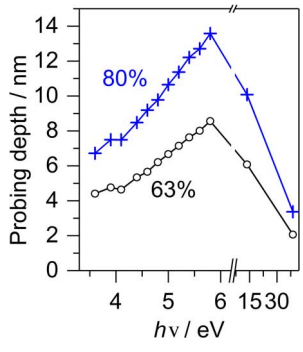

Fig. 4. Energy-dependent probing depth of e_{aq}^-. Probing depths as a function of the ionization laser energy $h\nu$. Black circles, probing depth corresponding to 63% of the total electron signal; blue crosses, probing depth corresponding to 80% of the total electron signal.

CONCLUSIONS

The unknown contribution of electron scattering to key properties of e_{aq}^- has led to controversial discussions in the past. Our detailed analysis has now revealed the existence of a distinct genuine $eBE^{(g)}$ spectrum and $PAD^{(g)}$ for e_{aq}^-. The result of this work provides the missing link between experimentally measurable quantities and genuine properties. The merit of the latter, that is, of properties undistorted by scattering, is twofold. They are independent of experimental conditions so that they can be directly compared between different experiments resolving ambiguities in the determination of hydrated electron properties. As an additional advantage, genuine properties offer the possibility of a straightforward comparison with quantum chemical calculations (*13*), for example, to provide insight into the origin of the shape of the $eBE^{(g)}$ spectrum. Of particular relevance to unraveling the role of e_{aq}^- in radiation and aqueous solution chemistry (*1*–*4*) is the extension of scattering cross sections to very low kinetic energies for liquid water.

MATERIALS AND METHODS

The experimental photoelectron spectra of the hydrated electron in the liquid water microjet were recorded with a magnetic bottle photoelectron spectrometer after formation of the hydrated electron by CTTS excitation (see section S3 for details) (*8*, *23*). The calculated photoelectron spectra were based on detailed electron scattering simulations using a Monte Carlo solution of the transport equations (*35*). The initial spatial distribution of photoelectrons was obtained from the light intensity distribution across the profile of the liquid jet, which we calculated from the wavelength-dependent complex index of refraction of water by numerically solving Maxwell's equations. For a given $h\nu$, the choice of $eBE^{(g)}$ spectrum and anisotropy $\beta^{(g)}$ then determined the initial velocity distribution of the photoelectrons. Their subsequent transport through the liquid consisted of a random succession of scattering events until the electrons were either absorbed or left the jet and were detected. The differential scattering cross sections end electron loss parameters by Signorell *et al.* and Michaud *et al.* (*35*, *39*) were used for the description of elastic and all different types of inelastic scattering (see section S2 for details). Integral scattering cross sections for liquid water at low eKEs are provided in fig. S3. The $eBE^{(g)}$ spectrum shown in Fig. 3 was obtained by maximizing the cross-correlation between the complete set of experimental and simulated eKE spectra. We performed an explicit sensitivity analysis to derive the quoted uncertainties of the final result (see section S6 and fig. S10 for details).

SUPPLEMENTARY MATERIALS

Supplementary material for this article is available at http://advances.sciencemag.org/cgi/content/full/3/4/e1603224/DC1

SupplementaryText

Supplementary Materials and Methods

section S1. Experimental values for the VBE of the bulk hydrated electron

section S2. Description of scattering calculations

section S3. Description of experimental setup

section S4. Additional eKE distributions

section S5. Sensitivity of eKE distributions to scattering parameters

section S6. Additional electron binding energy spectra

section S7. Probing depth and surface sensitivity

section S8. Photoelectron angular distribution

table S1. Previously reported values of the VBEs for the bulk hydrated electron.

fig. S1. Experimental VBEs by Yamamoto *et al.* (*8*).

fig. S2. Light intensity distribution in the liquid microjet.

fig. S3. Integral scattering cross sections for electrons in water as a function of the eKE as derived by Signorell *et al.* and Michaud *et al.* (*35*, *39*).

fig. S4. Scheme of the experimental setup.

fig. S5. Direct comparison of the experimental and calculated photoelectron kinetic energy distributions from Fig. 2 for all probe energies $h\nu$.

fig. S6. The influence of scattering on the eKE distributions.

fig. S7. Sensitivity of eKE distributions to an increase in the inelastic mean free path (IMFP) of +40%, which corresponds to the upper uncertainty limit of the IMFP (*35*).

fig S8. Sensitivity of eKE distributions to a change in the angular distribution of the inelastic scattering events (section S2).

fig. S9. Experimental eBE spectra for the different photon energies between 3.6 eV ≤ $h\nu$ ≤ 13.6 eV.

fig. S10. Uncertainty of the $eBE^{(g)}$ spectrum.

fig. S11. Fraction of the total electron intensity that originates from cylindrical shells of various thickness for photon energies 3.6 eV ≤ $h\nu$ ≤ 13.6 eV and for a photon energy $h\nu$ = 38.7 eV (red, dashed line) (*6*).

fig. S12. Surface contribution to the eBE spectra for (A) $h\nu$ = 3.6 eV and (B) $h\nu$ = 5.8 eV.

fig. S13. Calculated angle-dependent liquid jet photoelectron spectra for different ionization laser polarization directions 0° ≤ θ ≤ 90° (section S2 and fig. S4) and a photon energy of $h\nu$ = 4.8 eV (*23*).

fig. S14. Calculated velocity map photoelectron image for hydrated electrons in an anion cluster with ~50 H_2O molecules for a genuine anisotropy parameter $\beta^{(g)}$ = 0.6 and a photon energy of $h\nu$ = 3.1 eV (*45*).

References (*47*–*57*)

REFERENCES AND NOTES

1. B. C. Garrett, D. A. Dixon, D. M. Camaioni, D. M. Chipman, M. A. Johnson, C. D. Jonah, G. A. Kimmel, J. H. Miller, T. N. Rescigno, P. J. Rossky, S. S. Xantheas, S. D. Colson, A. H. Laufer, D. Ray, P. F. Barbara, D. M. Bartels, K. H. Becker, K. H. Bowen, S. E. Bradforth, I. Carmichael, J. V. Coe, L. R. Corrales, J. P. Cowin, M. Dupuis, K. B. Eisenthal, J. A. Franz, M. S. Gutowski, K. D. Jordan, B. D. Kay, J. A. LaVerne, S. V. Lymar, T. E. Madey, C. W. McCurdy, D. Meisel, S. Mukamel, A. R. Nilsson, T. M. Orlando, N. G. Petrik, S. M. Pimblott, J. R. Rustad, G. K. Schenter, S. J. Singer, A. Tokmakoff, L.-S. Wang, C. Wittig, T. S. Zwier, Role of water in electron-initiated processes and radical chemistry: Issues and scientific advances. *Chem. Rev.* **105**, 355–390 (2005).
2. E. Alizadeh, L. Sanche, Precursors of solvated electrons in radiobiological physics and chemistry. *Chem. Rev.* **112**, 5578–5602 (2012).
3. E. Alizadeh, T. M. Orlando, L. Sanche, Biomolecular damage induced by ionizing radiation: The direct and indirect effects of low-energy electrons on DNA. *Annu. Rev. Phys. Chem.* **66**, 379–398 (2015).
4. B. Abel, Hydrated interfacial ions and electrons. *Annu. Rev. Phys. Chem.* **64**, 533–552 (2013).
5. Y. Tang, H. Shen, K. Sekiguchi, N. Kurahashi, T. Mizuno, Y.-I. Suzuki, T. Suzuki, Direct measurement of vertical binding energy of a hydrated electron. *Phys. Chem. Chem. Phys.* **12**, 3653–3655 (2010).
6. K. R. Siefermann, Y. X. Liu, E. Lugovoy, O. Link, M. Faubel, U. Buck, B. Winter, B. Abel, Binding energies, lifetimes and implications of bulk and interface solvated electrons in water. *Nat. Chem.* **2**, 274–279 (2010).
7. A. T. Shreve, T. A. Yen, D. M. Neumark, Photoelectron spectroscopy of hydrated electrons. *Chem. Phys. Lett.* **493**, 216–219 (2010).
8. Y.-i. Yamamoto, S. Karashima, S. Adachi, T. Suzuki, Wavelength dependence of UV photoemission from solvated electrons in bulk water, methanol, and ethanol. *J. Phys. Chem. A* **120**, 1153–1159 (2016).
9. D. M. Sagar, C. D. Bain, J. R. R. Verlet, Hydrated electrons at the water/air interface. *J. Am. Chem. Soc.* **132**, 6917–6919 (2010).
10. J. M. Herbert, M. P. Coons, The hydrated electron. *Annu. Rev. Phys. Chem.* **68**, (2017).
11. J. M. Herbert, L. D. Jacobson, Structure of the aqueous electron: Assessment of one-electron pseudopotential models in comparison to experimental data and time-dependent density functional theory. *J. Phys. Chem. A* **115**, 14470–14483 (2011).
12. L. D. Jacobson, J. M. Herbert, A one-electron model for the aqueous electron that includes many-body electron-water polarization: Bulk equilibrium structure, vertical electron binding energy, and optical absorption spectrum. *J. Chem. Phys.* **133**, 154506 (2010).
13. M. P. Coons, Z.-Q. You, J. M. Herbert, The hydrated electron at the surface of neat liquid water appears to be indistinguishable from the bulk species. *J. Am. Chem. Soc.* **138**, 10879–10886 (2016).
14. J. R. Casey, B. J. Schwartz, W. J. Glover, Free energies of cavity and noncavity hydrated electrons near the instantaneous air/water interface. *J. Phys. Chem. Lett.* **7**, 3192–3198 (2016).
15. F. Uhlig, O. Marsalek, P. Jungwirth, Unraveling the complex nature of the hydrated electron. *J. Phys. Chem. Lett.* **3**, 3071–3075 (2012).
16. F. Uhlig, O. Marsalek, P. Jungwirth, Electron at the surface of water: Dehydrated or not? *J. Phys. Chem. Lett.* **4**, 338–343 (2013).
17. R. E. Larsen, W. J. Glover, B. J. Schwartz, Does the hydrated electron occupy a cavity? *Science* **329**, 65–69 (2010).

18. R. M. Young, D. M. Neumark, Dynamics of solvated electrons in clusters. *Chem. Rev.* **112**, 5553–5577 (2012).
19. K. R. Asmis, G. Santambrogio, J. Zhou, E. Garand, J. Headrick, D. Goebbert, M. A. Johnson, D. M. Neumark, Vibrational spectroscopy of hydrated electron clusters $(H_2O)^-_{15-50}$ via infrared multiple photon dissociation. *J. Chem. Phys.* **126**, 191105 (2007).
20. J. V. Coe, G. H. Lee, J. G. Eaton, S. T. Arnold, H. W. Sarkas, K. H. Bowen, C. Ludewigt, H. Haberland, D. R. Worsnop, Photoelectron spectroscopy of hydrated electron cluster anions, $(H_2O)^-_{n=2-69}$. *J. Chem. Phys.* **92**, 3980–3982 (1990).
21. L. Ma, K. Majer, F. Chirot, B. von Issendorff, Low temperature photoelectron spectra of water cluster anions. *J. Chem. Phys.* **131**, 144303 (2009).
22. S. Karashima, Y. Yamamoto, T. Suzuki, Resolving nonadiabatic dynamics of hydrated electrons using ultrafast photoemission anisotropy. *Phys. Rev. Lett.* **116**, 137601 (2016).
23. Y.-i. Yamamoto, Y.-I. Suzuki, G. Tomasello, T. Horio, S. Karashima, R. Mitric, T. Suzuki, Time- and angle-resolved photoemission spectroscopy of hydrated electrons near a liquid water surface. *Phys. Rev. Lett.* **112**, 187603 (2014).
24. M. H. Elkins, H. L. Williams, A. T. Shreve, D. M. Neumark, Relaxation mechanism of the hydrated electron. *Science* **342**, 1496–1499 (2013).
25. M. H. Elkins, H. L. Williams, D. M. Neumark, Isotope effect on hydrated electron relaxation dynamics studied with time-resolved liquid jet photoelectron spectroscopy. *J. Chem. Phys.* **144**, 184503 (2016).
26. T. W. Kee, D. H. Son, P. Kambhampati, P. F. Barbara, A unified electron transfer model for the different precursors and excited states of the hydrated electron. *J. Phys. Chem. A* **105**, 8434–8439 (2001).
27. A. Lübcke, F. Buchner, N. Heine, I. V. Hertel, T. Schultz, Time-resolved photoelectron spectroscopy of solvated electrons in aqueous NaI solution. *Phys. Chem. Chem. Phys.* **12**, 14629–14634 (2010).
28. F. Buchner, T. Schultz, A. Lübcke, Solvated electrons at the water-air interface: Surface versus bulk signal in low kinetic energy photoelectron spectroscopy. *Phys. Chem. Chem. Phys.* **14**, 5837–5842 (2012).
29. A. Kothe, M. Wilke, A. Moguilevski, N. Engel, B. Winter, I. Y. Kiyan, E. F. Aziz, Charge transfer to solvent dynamics in iodide aqueous solution studied at ionization threshold. *Phys. Chem. Chem. Phys.* **17**, 1918–1924 (2015).
30. J. Savolainen, F. Uhlig, S. Ahmed, P. Hamm, P. Jungwirth, Direct observation of the collapse of the delocalized excess electron in water. *Nat. Chem.* **6**, 697–701 (2014).
31. X. Chen, S. E. Bradforth, The ultrafast dynamics of photodetachment. *Annu. Rev. Phys. Chem.* **59**, 203–231 (2008).
32. Á. Madarász, P. J. Rossky, L. Turi, Excess electron relaxation dynamics at water/air interfaces. *J. Chem. Phys.* **126**, 234707 (2007).
33. K. Matsuzaki, R. Kusaka, S. Nihonyanagi, S. Yamaguchi, T. Nagata, T. Tahara, Partially hydrated electrons at the air/water interface observed by UV-excited time-resolved heterodyne-detected vibrational sum frequency generation spectroscopy. *J. Am. Chem. Soc.* **138**, 7551–7557 (2016).
34. Y. Tang, Y.-i. Suzuki, H. Shen, K. Sekiguchi, N. Kurahashi, K. Nishizawa, P. Zuo, T. Suzuki, Time-resolved photoelectron spectroscopy of bulk liquids at ultra-low kinetic energy. *Chem. Phys. Lett.* **494**, 111–116 (2010).
35. R. Signorell, M. Goldmann, B. L. Yoder, A. Bodi, E. Chasovskikh, L. Lang, D. Luckhaus, Nanofocusing, shadowing, and electron mean free path in the photoemission from aerosol droplets. *Chem. Phys. Lett.* **658**, 1–6 (2016).
36. S. Thürmer, R. Seidel, M. Faubel, W. Eberhardt, J. C. Hemminger, S. E. Bradforth, B. Winter, Photoelectron angular distributions from liquid water: Effects of electron scattering. *Phys. Rev. Lett.* **111**, 173005 (2013).
37. C. Zhang, T. Andersson, M. Förstel, M. Mucke, T. Arion, M. Tchaplyguine, O. Björneholm, U. Hergenhahn, The photoelectron angular distribution of water clusters. *J. Chem. Phys.* **138**, 234306 (2013).
38. I. Plante, F. A. Cucinotta, Cross sections for the interactions of 1 eV–100 MeV electrons in liquid water and application to Monte-Carlo simulation of HZE radiation tracks. *New J. Phys.* **11**, 063047 (2009).
39. M. Michaud, A. Wen, L. Sanche, Cross sections for low-energy (1–100 eV) electron elastic and inelastic scattering in amorphous ice. *Radiat. Res.* **159**, 3–22 (2003).
40. N. Ottosson, M. Faubel, S. E. Bradforth, P. Jungwirth, B. Winter, Photoelectron spectroscopy of liquid water and aqueous solution: Electron effective attenuation lengths and emission-angle anisotropy. *J. Electron Spectrosc. Relat. Phenom.* **177**, 60–70 (2010).
41. Y.-I. Suzuki, K. Nishizawa, N. Kurahashi, T. Suzuki, Effective attenuation length of an electron in liquid water between 10 and 600 eV. *Phys. Rev. E* **90**, 010302 (2014).
42. C.-C. Su, Y. Yu, P.-C. Chang, Y.-W. Chen, I.-Y. Chen, Y.-Y. Lee, C. C. Wang, VUV photoelectron spectroscopy of cysteine aqueous aerosols: A microscopic view of its nucleophilicity at varying pH conditions. *J. Phys. Chem. Lett.* **6**, 817–823 (2015).
43. N. Kurahashi, S. Karashima, Y. Tang, T. Horio, B. Abulimiti, Y.-I. Suzuki, Y. Ogi, M. Oura, T. Suzuki, Photoelectron spectroscopy of aqueous solutions: Streaming potentials of NaX (X = Cl, Br, and I) solutions and electron binding energies of liquid water and X^-. *J. Chem. Phys.* **140**, 174506 (2014).
44. G. Olivieri, A. Goel, A. Kleibert, D. Cvetko, M. A. Brown, Quantitative ionization energies and work functions of aqueous solutions. *Phys. Chem. Chem. Phys.* **18**, 29506–29515 (2016).
45. A. E. Bragg, J. R. R. Verlet, A. Kammrath, O. Cheshnovsky, D. M. Neumark, Electronic relaxation dynamics of water cluster anions. *J. Am. Chem. Soc.* **127**, 15283–15295 (2005).
46. J. Bernasconi, E. Cartier, P. Pfluger, Hot-electron transport through thin dielectric films: Boltzmann theory and electron spectroscopy. *Phys. Rev. B* **38**, 12567–12581 (1988).
47. A. T. Shreve, M. H. Elkins, D. M. Neumark, Photoelectron spectroscopy of solvated electrons in alcohol and acetonitrile microjets. *Chem. Sci.* **4**, 1633–1639 (2013).
48. T. Horio, H. Shen, S. Adachi, T. Suzuki, Photoelectron spectra of solvated electrons in bulk water, methanol, and ethanol. *Chem. Phys. Lett.* **535**, 12–16 (2012).
49. H. Hayashi, N. Hiraoka, Accurate measurements of dielectric and optical functions of liquid water and liquid benzene in the VUV region (1–100 eV) using small-angle inelastic x-ray scattering. *J. Phys. Chem. B* **119**, 5609–5623 (2015).
50. Lumerical Solutions Inc., FDTD Solutions; www.lumerical.com.
51. M. Goldmann, J. Miguel-Sánchez, A. H. C. West, B. L. Yoder, R. Signorell, Electron mean free path from angle-dependent photoelectron spectroscopy of aerosol particles. *J. Chem. Phys.* **142**, 224304 (2015).
52. A. Manka, H. Pathak, S. Tanimura, J. Wölk, R. Strey, B. E. Wyslouzil, Freezing water in no-man's land. *Phys. Chem. Chem. Phys.* **14**, 4505–4516 (2012).
53. J. D. Smith, C. D. Cappa, W. S. Drisdell, R. C. Cohen, R. J. Saykally, Raman thermometry measurements of free evaporation from liquid water droplets. *J. Am. Chem. Soc.* **128**, 12892–12898 (2006).
54. C. G. Elles, A. E. Jailaubekov, R. A. Crowell, S. E. Bradforth, Excitation-energy dependence of the mechanism for two-photon ionization of liquid H_2O and D_2O from 8.3 to 12.4 eV. *J. Chem. Phys.* **125**, 044515 (2006).
55. J. V. Coe, A. D. Earhart, M. H. Cohen, G. J. Hoffman, H. W. Sarkas, K. H. Bowen, Using cluster studies to approach the electronic structure of bulk water: Reassessing the vacuum level, conduction band edge, and band gap of water. *J. Chem. Phys.* **107**, 6023–6031 (1997).
56. T. Suzuki, Time-resolved photoelectron spectroscopy of non-adiabatic electronic dynamics in gas and liquid phases. *Int. Rev. Phys. Chem.* **31**, 265–318 (2012).
57. G. Olivieri, K. M. Parry, C. J. Powell, D. J. Tobias, M. A. Brown, Quantitative interpretation of molecular dynamics simulations for X-ray photoelectron spectroscopy of aqueous solutions. *J. Chem. Phys.* **144**, 154704 (2016).

Acknowledgments

Funding: This research is supported by the Swiss National Science Foundation (under grant 200020_159205), the ETH Zurich, and the Japan Society for the Promotion of Science (JSPS) KEKENHI (grant no. 15H05753). Y-i.Y. is supported by a Research Fellowship for Young Scientists awarded by the JSPS. **Author contribution:** R.S. and T.S. conceived the research project. T.S. and Y-i.Y. performed the liquid jet measurements. D.L. and R.S designed the model and performed the calculations. R.S. wrote the manuscript. **Competing interests:** The authors declare that they have no competing interests. **Data and materials availability:** All data needed to evaluate the conclusions in the paper are present in the paper and/or the Supplementary Materials. Additional data related to this paper may be requested from the authors.

Submitted 19 December 2016
Accepted 2 March 2017
Published 28 April 2017
10.1126/sciadv.1603224

Citation: D. Luckhaus, Y.-i. Yamamoto, T. Suzuki, R. Signorell, Genuine binding energy of the hydrated electron. *Sci. Adv.* **3**, e1603224 (2017).

Genuine binding energy of the hydrated electron

David Luckhaus, Yo-ichi Yamamoto, Toshinori Suzuki and Ruth Signorell

Sci Adv **3** (4), e1603224.
DOI: 10.1126/sciadv.1603224